J. Fluid Mech. (2012), *vol.* 713, *pp.* 1–26. © Cambridge University Press 2012
doi:10.1017/jfm.2012.423

A numerical study of granular shear flows of rod-like particles using the discrete element method

Y. Guo[1]†, C. Wassgren[2], W. Ketterhagen[3], B. Hancock[3], B. James[1] and J. Curtis[1]

[1] Chemical Engineering Department, University of Florida, Gainesville, FL 32611, USA

[2] School of Mechanical Engineering, Purdue University, West Lafayette, IN 47907, USA

[3] Pfizer, Inc., Groton, CT 06340, USA

(Received 21 February 2012; revised 9 July 2012; accepted 17 August 2012; first published online 12 October 2012)

The effect of particle aspect ratio and surface geometry on granular flows is assessed by performing numerical simulations of rod-like particles in simple shear flows using the discrete element method (DEM). The effect of particle surface geometry is explored by adopting two types of particles: glued-spheres particles and true cylindrical particles. The particle aspect ratio varies from one to six. Compared to frictionless spherical particles, smaller stresses are obtained for the glued-spheres and cylindrical particle systems in dilute and moderately dense flows due to the loss of translational energy, which is partially converted to rotational energy, for the non-spherical particles. For dilute granular flows of non-spherical particles, stresses are primarily affected by the particle aspect ratio rather than the surface geometry. As the particle aspect ratio increases, the effective particle projected area in the plane perpendicular to the flow direction increases, so that the probability of the occurrence of the particle collisions increases, leading to a reduction in particle velocity fluctuation and therefore a decrease in the stresses. Hence, a simple modification is made to the kinetic theory for granular flows to describe the stress tensors for dilute flows of non-spherical particles by incorporating a normalized effective particle projected area to account for the effect of particle collision probability. For dense granular flows, the stresses depend on both the particle aspect ratio and the surface geometry. Sharp stress increases at high solid volume fractions are observed for the glued-spheres particles with large aspect ratios due to the bumpy surfaces, which impede the flow. However, smaller stresses are obtained for the true cylindrical particles with large aspect ratios at high solid volume fractions. This trend is attributed to the combined effects of the smooth particle surfaces and the particle alignments such that the major/long axes of particles are aligned in the flow direction. In addition, the apparent friction coefficient, defined as the ratio of shear to normal stresses, is found to decrease as the particle aspect ratio increases and/or the particle surface becomes smoother at high solid volume fractions.

Key words: granular media, kinetic theory, multiphase flow

† Email address for correspondence: guoyu03@hotmail.com

https://doi.org/10.1017/jfm.2012.423 Published online by Cambridge University Press

1. Introduction

The flow of granular materials is widely found in natural phenomena (e.g. sand storms, debris flows and landslides) and in many powder-handling industries (e.g. pharmaceutical, powder metallurgy, mining and food industries). Therefore, it is not surprising that there is an extensive body of published and ongoing research work aimed at a better understanding of the underlying physics of granular flows (Campbell 2006; Jenkins 2006; Forterre & Pouliquen 2008), which will help reduce and avoid the damages from natural disasters and aid in the design and optimization of industrial processes.

A granular system is by nature a collection of individual solid particles. Each particle moves driven by a combination of external forces (e.g. gravitational force, interstitial fluid force, magnetic force, electric force, etc.) and contact forces due to the interaction with neighbouring particles. The overall flow behaviour of the granular system is a result of the motions of all particles. With this idea in mind, a computational approach, namely the discrete element method (DEM), was developed (Cundall & Strack 1979) and thereafter applied to investigation of a variety of granular flow situations (Campbell & Gong 1986, Walton & Braun 1986, Campbell 1989, Lasinski, Curtis & Pekny 2004, Ketterhagen, Curtis & Wassgren 2005). This method allows for the 'measurement' of many quantities, such as particle solid volume fraction, particle velocity, granular temperature, and stress tensors. However, due to the down-to-particle-size resolution, the computational cost associated with this method of simulation increases dramatically with the number of particles in the system. According to the experience of the authors and other DEM modellers (Cleary 2008), if the number of particles is above 10^7, one would be reluctant to carry out simulations using the DEM based on current computer capacity.

The most prevalent way to study a large-scale granular system is to treat it as a continuum, and adopt methods normally used to investigate continua. Granular kinetic theory is one such method, and was introduced to describe dilute and moderately dense granular flows in which the motion of individual particles is analogous to the thermal motion of molecules in gases, and the particle–particle collisions are binary and instantaneous (Lun *et al.* 1984; Goldshtein & Shapiro 1995; Montanero *et al.* 1999). This method yields a set of Navier–Stokes-like equations to ensure the conservation of mass and momentum (Campbell 2006).

According to a kinetic theory model by Lun *et al.* (1984), the normal and shear stresses in plane shear flows of smooth, hard and inelastic spheres can be written as follows:

$$\sigma_{yy} = \sigma_{xx} = \sigma_{zz} = \rho\nu T(1 + 4\eta\nu g_0), \tag{1.1}$$

$$\sigma_{xy} = \sigma_{yx} = -\tfrac{5}{96} F(\nu, e)\rho\,(\pi T)^{1/2}\, d_p\gamma \tag{1.2}$$

where the granular temperature T can be expressed as

$$T = \frac{5\pi}{4608}\,\frac{F(\nu, e)}{\eta(1-\eta)\nu^2 g_0}\, d_p^2\gamma^2, \tag{1.3}$$

and $F(\nu, e)$ has the form

$$F(\nu, e) = \frac{1}{\eta(2-\eta)g_0}\left(1 + \frac{8}{5}\eta\nu g_0\right)\left[1 + \frac{8}{5}\eta\nu g_0(3\eta - 2)\right] + \frac{768}{25\pi}\eta\nu^2 g_0. \tag{1.4}$$

In the above relations, ρ is the material density of the particle, d_p is the particle diameter, γ is the applied shear rate, ν is the solid volume fraction, e represents the

https://doi.org/10.1017/jfm.2012.423 Published online by Cambridge University Press

coefficient of restitution, η is a function of e,

$$\eta = \tfrac{1}{2}(1+e), \tag{1.5}$$

and g_0 is the radial distribution function for a pair of contacting spheres. According to Carnahan & Starling (1969), g_0 solely depends on ν as

$$g_0(\nu) = \frac{1}{1-\nu} + \frac{3\nu}{2\,(1-\nu)^2} + \frac{\nu^2}{2\,(1-\nu)^3}. \tag{1.6}$$

The stresses, as expressed in (1.1) and (1.2), can be normalized using $\rho d_p^2\gamma^2$ to become dimensionless. By substituting (1.3) into (1.1) and (1.2), the normalized stresses can be finally written as a function of solid fraction (ν) and coefficient of restitution (e), as follows:

$$\sigma_{yy}^N(\nu, e) = \frac{\sigma_{yy}}{\rho d_p^2\gamma^2} = \frac{5\pi}{4608}\,\frac{F(\nu, e)}{\eta(1-\eta)\nu g_0}\,(1+4\eta\nu g_0), \tag{1.7}$$

$$\sigma_{xy}^N(\nu, e) = \frac{\sigma_{xy}}{\rho d_p^2\gamma^2} = -\frac{5\pi}{4608}\,\frac{F(\nu, e)}{\nu}\,\sqrt{\frac{5}{2}\frac{F(\nu, e)}{\eta(1-\eta)g_0}}. \tag{1.8}$$

It should be noted that only translational momentum and energy transport occur in the systems of smooth disks or spheres due to the absence of tangential interaction. If the particles have rough surfaces, the frictional forces can cause the rotation of particles, causing translational energy to be converted to rotational energy and heat when sliding occurs at the contact points. This effect will also have an impact on the flow behaviour. In fact, significant attempts have been made to develop the kinetic theories for frictional disks (Jenkins & Richman 1985; Yoon & Jenkins 2005) and frictional spheres (Jenkins & Zhang 2002). To consider the additional loss of translational energy to friction and particle rotation, these authors proposed an effective coefficient of normal restitution, e_{eff}, which can be approximately described as a function of the real coefficient of normal restitution, e, and the friction coefficient, μ. The resulting theories for frictional disks and spheres can be obtained simply by using e_{eff} to replace e in the theories for smooth ones.

In dense granular flows, the multiple long-lasting collisions become dominant and consequently force chains are formed to oppose the flows (Campbell 2002, 2005; Jenkins 2006). As a result, the kinetic theory, established on the assumption of binary, instantaneous collisions, cannot be directly used to capture the features of dense flows. Jenkins (2006) modified the hydrodynamic equations for dense flows of frictionless, inelastic disks by incorporating a length scale in the expression of the rate of collisional dissipation. Johnson & Jackson (1987) and Johnson, Nott & Jackson (1990) suggested adding a frictional contribution to the stress from the kinetic theory, and following this idea, Berzi, di Prisco & Vescovi (2011) proposed a formalism of the frictional component in which the role of the particle contact stiffness is considered. Campbell (2002, 2005, 2006) also recognized the importance of the elastic properties of particles in determining the overall rheology of dense granular flows. In his studies, the dimensionless stresses $\sigma d_p/k$ were plotted against the dimensionless stiffness $k/(\rho d_p^3\gamma^2)$ (where k represents the interparticle contact stiffness). The results showed that the stresses scale with the stiffness, indicating that the stresses are generated by the particle elasticity. Moreover, two regimes are distinguished for dense granular flows: the elastic-inertial regime, in which the stresses scale elastically and

https://doi.org/10.1017/jfm.2012.423 Published online by Cambridge University Press

increase linearly with shear rate, and the elastic-quasi-static regime, in which the stresses again scale elastically, but are independent of strain rate.

Most of the early studies on granular shear flows were conducted using simple shapes for the particles such as circular disks or spheres. However, recent works (Peña, García-Rojo & Herrmann 2007; Cleary 2008; Reddy, Kumaran & Talbot 2009; Reddy, Talbot & Kumaran 2010; Campbell 2011) reveal that the shape of the particles has a significant impact on the shear flow behaviour of granular materials. Two-dimensional DEM simulations were performed for dense plane Couette flows with polygonal disks by Peña *et al.* (2007) and with circular, squarish, and elliptical disks by Cleary (2008), and they found that the increase in non-circularity of the particles (by increasing their aspect ratios and/or making them more angular/blocky) leads to a sharp increase in the strength of the material, making it harder to shear. This result was attributed to the interlocking of the blocky particles. In addition, the generation of particle rotation throughout the flow of blocky or elliptical particles causes large granular temperatures and smaller solid fractions in the core of the flow.

A significant feature in granular shear flows of non-spherical particles is that the elongated particles have a preferred alignment such that the major axis (long axis) is inclined at a typical angle with respect to the main flow stream, as observed by Peña *et al.* (2007), Reddy *et al.* (2009, 2010), and Campbell (2011). In order to quantify the degree of this orientational alignment, Reddy *et al.* (2009, 2010) proposed an order parameter, which varies between 0 (for a randomly orientated particle system) and 1 (for a system with the major axes of all particles in the same direction). According to their two-dimensional hard-particle simulation studies of sheared inelastic dumbbells, which are formed by rigidly connecting two circular disks, it was found that the order parameter, i.e. the tendency of particle alignment, increases as the particle aspect ratio (the ratio of particle length to the diameter of constituent sphere) increases, as the solid area fraction increases and/or the coefficient of restitution decreases. With the particle aspect ratios considered (i.e. in the range 1–2), the particle shape has much less influence on the stresses than the solid fraction. In addition, for the dense flows with elongated particles, although the stress tensor is symmetric, the mean angular velocity of particles is less than half the vorticity of the mean flow, indicating that the flow of anisotropic particles cannot be described by the existing continuum Cosserat theories (Reddy *et al.* 2010).

Recently, Campbell (2011), based on his three-dimensional DEM simulations of simple shear flows with ellipsoids, stated that due to the effect of particle alignment, the smoothed ellipsoidal particles are able to 'stay out of the way' of the flow paths of the neighbouring particles, minimizing the interference with the shear flow. Thus, smaller stresses were observed for ellipsoids than for spheres. However, when the ellipsoidal particles had large surface friction, the frictional forces drove the particles to rotate and block the flow. Consequently, the preferred alignment was weakened, and the force chains were formed at relatively smaller concentrations, causing larger stresses. It was also found that the friction had a stronger effect on the non-spherical particles than on the spherical particles.

Although significant progress has been made, our understanding of how particle shape influences granular flows is still largely lacking. In this paper, we developed a DEM model to investigate simple shear flows using three-dimensional rod-like particles formed by gluing spheres or using true cylinders, which have the particle aspect ratios in a wide range of 1–6. This approach enables us to explore the effect of particle shape (in terms of particle aspect ratio and surface roughness) on the flow behaviour and constitutive relations of stress tensors in granular shear flows.

https://doi.org/10.1017/jfm.2012.423 Published online by Cambridge University Press

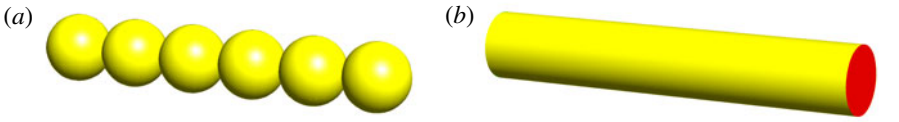


FIGURE 1. (Colour online) Representations of the rod-like particles. ($AR = 6$): (a) glued-spheres particle; (b) cylindrical particle.

2. Computational model

2.1. *Discrete element method*

Two representations of rod-like particles are generated in the current DEM model. As illustrated in figure 1, one is a glued-spheres particle, which is formed by rigidly connecting identical spheres in a straight line without gaps or overlaps; the other one is referred to as a cylindrical particle, which is a representation of a true cylinder with a cylindrical band and two flat end surfaces. The aspect ratio (AR), defined as the ratio of particle length to the diameter of the constituent sphere (for the glued-spheres particle) or circular face (for the cylindrical particle), indicates the degree of particle elongation. In this study, four different aspect ratios ($AR = 1$, 2, 4 and 6) are considered.

The translational and rotational motion of an individual particle i is governed by Newton's second law of motion as follows:

$$m_i \frac{\mathrm{d}\boldsymbol{v}_i}{\mathrm{d}t} = \boldsymbol{F}_i \tag{2.1}$$

and

$$\boldsymbol{I}_i \cdot \frac{\mathrm{d}\boldsymbol{\omega}_i}{\mathrm{d}t} - (\boldsymbol{I}_i \cdot \boldsymbol{\omega}_i) \times \boldsymbol{\omega}_i = \boldsymbol{T}_i \tag{2.2}$$

in which $\boldsymbol{v}_i$ and $\boldsymbol{\omega}_i$ are the translational and angular velocities, respectively, of the particle, and their derivatives with respect to the time t give the corresponding accelerations. The translational movement of the particle of mass m_i is driven by the resultant contact force $\boldsymbol{F}_i$, and the particle rotation is induced by the torque $\boldsymbol{T}_i$ arising from the contact forces. For the three-dimensional non-spherical particles, $\boldsymbol{I}_i$ represents the moment of inertia tensor. The evolution of velocities, positions and orientations of the individual particles can be obtained by the time integration of (2.1) and (2.2) using a central finite difference scheme with a fixed time step.

In this study, the particles are assumed to be frictionless. Therefore, no tangential force is present and only normal forces exist when interparticle contacts occur. The normal contact force is calculated based on the Hertz model (Hertz 1882):

$$F_n = \tfrac{4}{3} E^* R^{*1/2} \delta_n^{3/2}, \tag{2.3}$$

where

$$\frac{1}{E^*} = \frac{1-\nu_1^2}{E_1} + \frac{1-\nu_2^2}{E_2} \tag{2.4}$$

and

$$\frac{1}{R^*} = \frac{1}{R_1} + \frac{1}{R_2}, \tag{2.5}$$

https://doi.org/10.1017/jfm.2012.423 Published online by Cambridge University Press

and δ_n represents the overlap between the two particles in contact. In (2.4), E_1 and ν_1, and E_2 and ν_2 are the Young's moduli and Poisson's ratios, respectively, of two particles in contact. In (2.5), for the glued-spheres particles, R_1 and R_2 are the radii of the constituent spheres from two composite particles in contact, while for the cylindrical particles, R_1 and R_2 represent the radii of the circular end faces of two cylinders in contact.

To account for the kinetic energy dissipation due to the propagation of elastic waves, a damping force

$$F_n^d = 2\beta\sqrt{K_n m^*}V_n^r \tag{2.6}$$

is added to the normal contact force to provide the contribution to the out-of-balance force acting on the particle from that contact. In (2.6), V_n^r is the normal component of the relative velocity at the contact point, K_n is the contact stiffness, and $m^* = m_1 m_2/(m_1 + m_2)$, where m_1 and m_2 are the masses of two particles in contact. As indicated by Cleary & Sawley (2002), the damping coefficient β is a function of the coefficient of normal restitution e (defined as the ratio of the post-collisional to pre-collisional normal component of the relative velocity at the contact point):

$$\beta = -\frac{\ln e}{\sqrt{\pi^2 + \ln^2 e}}. \tag{2.7}$$

Therefore, the damping coefficient β can be chosen to give a required coefficient of normal restitution e for the modelling.

For the glued-spheres particles, the contacts are detected for each constituent sphere. A resultant force is obtained by summing the contact forces on all constituent spheres from a single particle, and a resultant torque is obtained by summing the torques arising from the contact forces with respect to the centre of the mass of the composite particle. For the cylindrical particles, the contact detection approach for the cylindrical objects proposed by Kodam *et al.* (2010*a*,*b*) and Guo *et al.* (2012) is employed to determine whether two particles are in contact, the degree of overlap, and the normal direction of contact.

2.2. *Numerical model of shear flow*

As shown in figure 2, a specified number of particles were generated in a domain (i.e. the cell in which the shear flow occurs), in which the particles are randomly positioned and the distribution of solid volume fraction is uniform. A procedure for the generation of a densely packed bed of elongated particles in a confined space is provided in our recent paper (Guo *et al.* 2012). The shear behaviour of the granular system was initiated by applying a linear x-velocity (V_x) profile in the y direction with zero velocity at the centre. If the dimension of the domain in the y direction is L, the applied shear strain rate can be expressed as $\gamma = 2U/L$. Periodic boundary conditions were applied in the x and z directions, and a Lees–Edwards boundary condition (Lees & Edwards 1972) was adopted in the y direction. During the shear flow process, no external forces (e.g. a gravitational force) were imposed on the particle system.

In this study, the particle equivalent sphere volume diameter (d_v), defined as the diameter of a sphere having the same volume as the non-spherical particle, is kept identical for all the glued-spheres and true cylindrical particles considered. In addition, the particles are assumed to be smooth, hard (having large contact stiffness), and slightly inelastic. The particle properties and simulation parameters are shown in table 1.

https://doi.org/10.1017/jfm.2012.423 Published online by Cambridge University Press

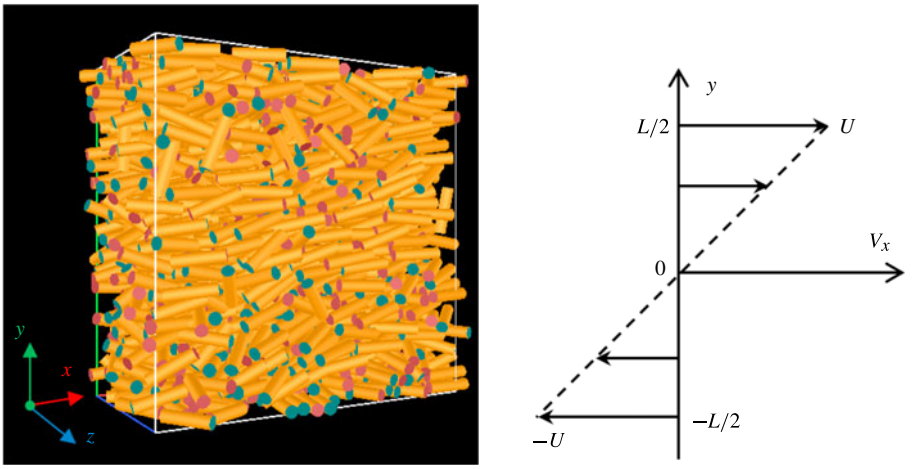


FIGURE 2. (Colour online) Numerical model of a granular shear flow of cylindrical particles.

Equivalent particle diameter d_v (m)	Particle density ρ (kg m^{-3})	Young's modulus E (Pa)	Poisson's ratio ν
4.762×10^{-4}	2500	8.7×10^9	0.3
Coefficient of restitution e	**Friction coefficient**	**Shear strain rate γ (s^{-1})**	**Time step (s)**
0.95	0.0	100	1.0^{-7}

TABLE 1. Particle properties and simulation parameters.

2.3. *Steady state stresses in shear flow*

The particle-phase stress tensor can be expressed as the sum of a kinetic or streaming component and a collisional component. Following Campbell & Gong (1986), the kinetic component, which arises from the momentum transfer by particles as they move through the bulk material, is given by

$$\boldsymbol{\sigma}_{kin} = \rho\nu\langle \boldsymbol{CC}\rangle, \tag{2.8}$$

in which $\langle\ \rangle$ represents an average over time and volume, and $\boldsymbol{C} = \boldsymbol{c}_i - \langle \boldsymbol{c}\rangle$ is the fluctuating velocity of particle i. The average velocity $\langle \boldsymbol{c}\rangle$ is the local steady state, shear velocity. The collisional component, which arises from the momentum transfer from one point to another in the material by interparticle collisions, is written as

$$\boldsymbol{\sigma}_{col} = \langle \boldsymbol{F}_i^j \boldsymbol{l}_{ic} + \boldsymbol{F}_j^i \boldsymbol{l}_{jc}\rangle, \tag{2.9}$$

where $\boldsymbol{F}_i^j$ is the contact force exerted on particle i by particle j, and $\boldsymbol{l}_{ic}$ is the vector pointing from the mass centre of particle i to the contact point. Similarly, $\boldsymbol{F}_j^i$ is the contact force exerted on particle j by particle i, and $\boldsymbol{l}_{jc}$ is the vector pointing from the mass centre of particle j to the contact point. For the contact between particles i and j,

https://doi.org/10.1017/jfm.2012.423 Published online by Cambridge University Press

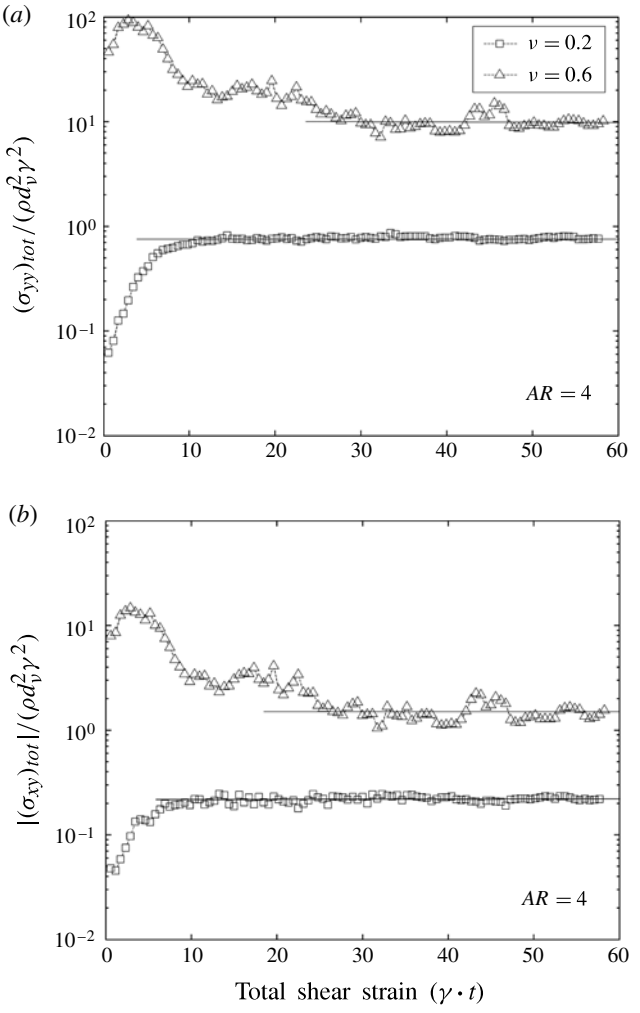


FIGURE 3. Time history of normal stresses (a) and shear stresses (b) in the shear flows of true cylindrical particles with $AR = 4$ and $\nu = 0.2$ and 0.6.

according to Newton's third law it gives $\boldsymbol{F}_j^i = -\boldsymbol{F}_i^j$, so that (2.9) can be rewritten as

$$\boldsymbol{\sigma}_{col} = \langle \boldsymbol{F}_i^j(\boldsymbol{l}_{ic} - \boldsymbol{l}_{jc})\rangle = \langle \boldsymbol{F}_i^j \boldsymbol{l}_{ij}\rangle, \tag{2.10}$$

in which $\boldsymbol{l}_{ij}$ represents the vector from the mass centre of particle i to the mass centre of particle j. In this study, the measurements of system stresses are made by calculating (2.8) and (2.10) and summing them.

In a simple shear flow of inelastic particles, the steady state is reached when there is a balance between the shear production (using the Lees–Edwards boundary condition in the present simulations) and the dissipation due to inelastic collisions. In figure 3, the normal and shear stresses, normalized by $\rho d_V^2\gamma^2$, are plotted as a function of total shear strain, which represents $\gamma\, t$ (i.e. the product of shear rate and elapsed time, t), for shear flows of true cylindrical particles with $AR = 4$ and $\nu = 0.2$ and 0.6. At the low solid volume fraction of $\nu = 0.2$, the stresses initially increase and then remain at

https://doi.org/10.1017/jfm.2012.423 Published online by Cambridge University Press

a nearly constant level referred to as the steady state stresses. During the early stage of shear flow, the fluctuating velocities of particles increase as more collisions occur, leading to an increase in stress. The stresses increase until steady state is reached. In contrast, for the high solid volume fraction case with $\nu = 0.6$, after a short period of increase, the stresses decrease significantly and finally remain at smaller stress levels with slight fluctuations. As will be discussed in detail later, at high solid volume fractions, the particles with large aspect ratios tend to rearrange such that the major axes align horizontally in the main flow direction as the shear flow proceeds. This particle alignment reduces the interference of the particles with the flow, leading to a decrease in the stresses. It is also observed that a longer time (larger total shear strain) is required for the shear flow to reach steady state, and greater fluctuations of stresses are obtained at higher solid volume fractions compared to lower solid fractions. In this paper, the stresses, except when stated otherwise, are the average stresses measured at steady state, which lasts for a total shear strain (i.e. $\gamma\, t$) of at least 20.

2.4. *Sensitivity to computational domain size*

With the Lees–Edwards and periodic boundary conditions, the computational domain should be sufficiently large to produce results independent of domain size, while simultaneously, a small domain size is preferable to minimize the computational cost. Therefore, before extensive simulation studies were performed, the dependence of the stress results on the computational domain size was checked by introducing two domains: a smaller one with particle equivalent diameter d_v scaled dimensions $[x, y, z]$ of [15.12, 15.12, 7.56], and a larger one with d_v scaled dimensions of [20.16, 20.16, 10.08]. The two different-sized domains using a variety of solid volume fractions and particle aspect ratios, and for both glued-spheres and true cylindrical particles, showed good agreement for both normal and shear stresses, and their kinetic and collisional components. Therefore, the smaller domain with the scaled dimensions of [15.12, 15.12, 7.56] was employed in the following simulations to reduce computational cost while still maintaining numerical accuracy. With the smaller domain, the required numbers of particles to achieve the solid volume fractions of 0.025, 0.05, 0.1, 0.2, 0.3, 0.4, 0.5 and 0.6 are 83, 166, 332, 664, 996, 1328, 1660 and 1992, respectively.

3. Results and discussion

In this section, the stress tensor results for shear flows with the glued-spheres and true cylindrical particles are first presented. Then, the effects of preferred particle orientation, particle projected area, and particle surface roughness on the stresses are discussed in detail. Lastly, the effect of particle shape on the apparent friction coefficient is examined.

3.1. *Stress tensors*

The kinetic components, collisional components, and total values of the normalized normal and shear stresses are plotted as a function of the solid volume fraction (ν) in figures 4–6, respectively. The predictions from granular kinetic theory (Lun *et al.* 1984) are also included to compare with the simulation results. It can be seen that granular kinetic theory can predict well the stresses and their components for the systems with smooth spheres ($AR = 1$), except at high solid fractions ($\nu > 0.4$). As discussed by Campbell (2002, 2005, 2006), the kinetic theory can be safely applied to the dilute and moderately dense systems in which binary, instantaneous collisions are dominant, but it might fail for dense systems where the multiple, long-lasting

https://doi.org/10.1017/jfm.2012.423 Published online by Cambridge University Press

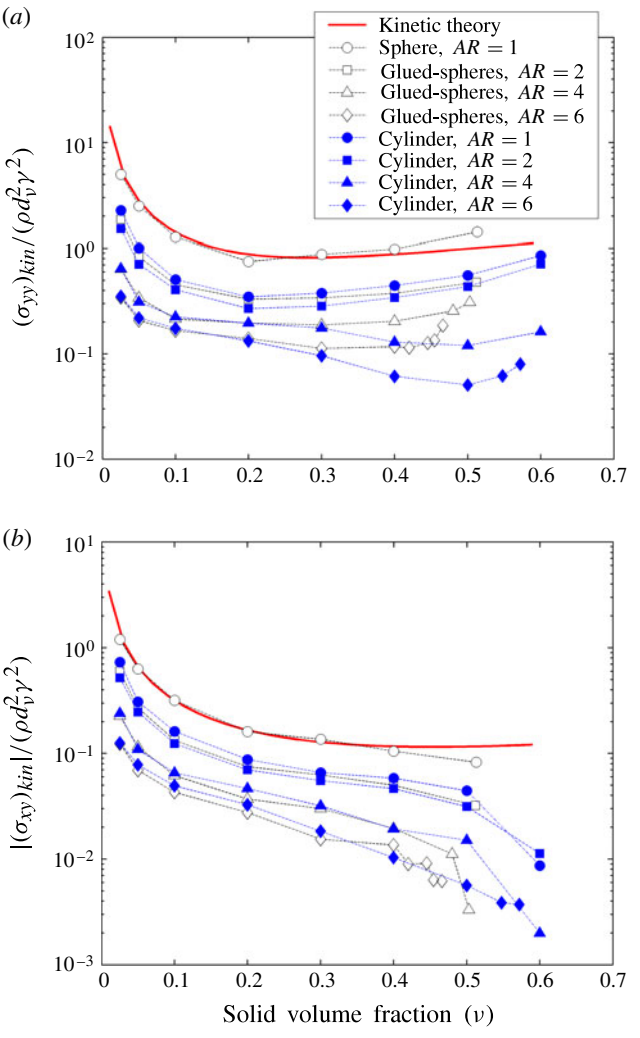


FIGURE 4. (Colour online) Kinetic components of the normalized normal stresses (*a*) and shear stresses (*b*) as a function of solid volume fraction (ν).

collisions become significant and the stresses show a dependence on the interparticle contact stiffness. This dependence on contact stiffness could explain the disagreement between the simulation results of the spheres and the kinetic theory at the high solid fractions.

As shown in figure 4(*a*), the kinetic normal stress for the glued-spheres and true cylindrical particles of various aspect ratios follows a similar trend to that for the spheres: the stress component initially decreases and then increases slightly with increasing ν. The initial quick decrease in the kinetic stresses can be attributed to the decrease in the mean free path, i.e. the distance travelled by a particle between two consecutive collisions, caused by the increase in concentration. The slight increase at high solid fractions may be the result of an increase in the fluctuation of the velocities perpendicular to the flow direction due to the more frequent collisions in

https://doi.org/10.1017/jfm.2012.423 Published online by Cambridge University Press

dense systems. The kinetic shear stress trends, as shown in figure 4(*b*), also follow a similar trend, with the stress component decreasing continuously with increasing ν.

The kinetic normal and shear stresses with the non-spherical particles (glued-spheres and true cylindrical particles) are generally smaller than those with the smooth spheres, as shown in figure 4(*a*,*b*). After interparticle collisions, the non-spherical particles rotate, due to the fact that the contact force vectors do not necessarily pass through the mass centres of the particles, and moments are generated to rotate the particles. As a result, part of the translational energy is converted to rotational energy. This conversion increases the rate of loss of the translational energy, leading to a decrease in the kinetic stresses. It is also observed that the kinetic normal and shear stresses decrease as the particle aspect ratio (AR) increases. This effect occurs because an increase in particle aspect ratio, under the condition of maintaining a fixed particle volume, requires an increase in the particle length along the major axis, which increases the chance for the particles to come into contact, decreases the mean free path, and also facilitates particle rotation.

Despite the difference in the surface geometry between the glued-spheres particles and the true cylindrical particles, nearly the same kinetic stresses are obtained for the glued-spheres and cylindrical particles with $AR = 2$ (figure 4*a*,*b*). However, with the larger particle aspect ratios of $AR = 4$ and 6, the same kinetic stresses are obtained at the low solid volume fractions (approximately $\nu < 0.3$) for the glued-spheres and cylindrical particles, but a difference in stress is obtained at the higher solid fractions.

For the collisional stresses, as shown in figure 5, the stress trends for the glued-spheres and cylindrical particles with small particle aspect ratios ($AR = 1$ and 2) follow the same trend as that for the spheres, with the collisional stresses increasing steadily with the solid volume fraction as particle collisions occur more frequently. For the glued-spheres particles with large aspect ratios ($AR = 4$ and 6), sharp increases in the collisional stresses are observed at the higher solid fractions ($0.4 < \nu < 0.5$). This behaviour may be due to the combined effects of the bumpy surfaces of the glued-spheres particles and the large particle length with the large aspect ratios. In a dense granular flow, the particles generally move by sliding over neighbouring particles. Under this condition, the bumpy and uneven surfaces of the glued-spheres particles can hinder the flow. In addition, the longer particles have a stronger influence on the flow of the granular material when they are rotated in the flow stream by interparticle contacts. As a result, the collisional stresses increase sharply for the glued-spheres particles with the large particle aspect ratios at high solid fractions. For true cylindrical particles with large aspect ratios ($AR = 4$ and 6), after the initial increase, the collisional stresses level off at intermediate solid volume fractions ($0.3 < \nu < 0.5$) and then begin to increase again with increasing solid volume fraction ($\nu > 0.5$). In shear flows, the large aspect ratio particles have a preferred orientation with their major axes aligned in the flow direction, as will be discussed below. This preferred alignment of particles minimizes the interaction between the particles and the bulk flow. In addition, the true cylindrical particles with large aspect ratios have long, smooth bands, which facilitate one particle sliding over another and reduce the chance for the particles to be interlocked. Due to the effects of particle alignment and smooth surface, in a moderately dense granular system ($\nu > 0.3$) lower collisional stresses are obtained for true cylindrical particles with large aspect ratios ($AR = 4$ and 6) compared to those with small aspect ratios of $AR = 1$ and 2 and to glued-spheres particles which have rough surfaces. However, as the solid volume fraction gets sufficiently large ($\nu > 0.5$), the space for the motion of a particle is confined, resulting in an increase in contact number and contact forces. Therefore, the collisional stresses increase again

https://doi.org/10.1017/jfm.2012.423 Published online by Cambridge University Press

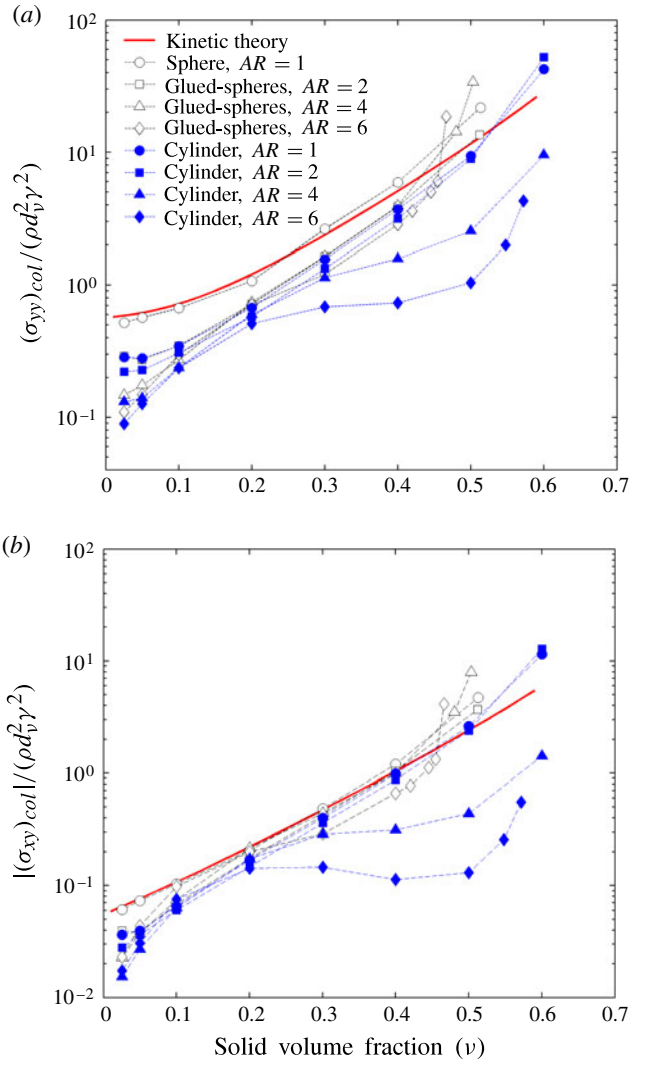


FIGURE 5. (Colour online) Collisional components of the normalized normal stresses (*a*) and shear stresses (*b*) as a function of solid volume fraction (ν).

with increasing solid volume fraction at high solid fractions for the cylindrical particles with large aspect ratios.

The total normal and shear stresses, which are the sum of the kinetic and collisional components, are plotted in figure 6. By comparing the total stress trends with the trends of their kinetic and collisional components as shown in figures 4 and 5, three distinct regimes can be classified. First is the dilute regime ($\nu < 0.1$ for $AR = 1$ and 2; $\nu < 0.05$ for $AR = 4$ and 6), in which the kinetic stresses are dominant and momentum is transferred mainly by particle motion. Therefore, the trends of total stresses in this regime follow the same shape as their kinetic components. Second is the dense regime ($\nu > 0.2$), in which the collisional stresses are dominant and the momentum is transferred mainly by interparticle collisions. Therefore, the trends of total stresses in this regime follow the same shape as their collisional components. Third is the

https://doi.org/10.1017/jfm.2012.423 Published online by Cambridge University Press

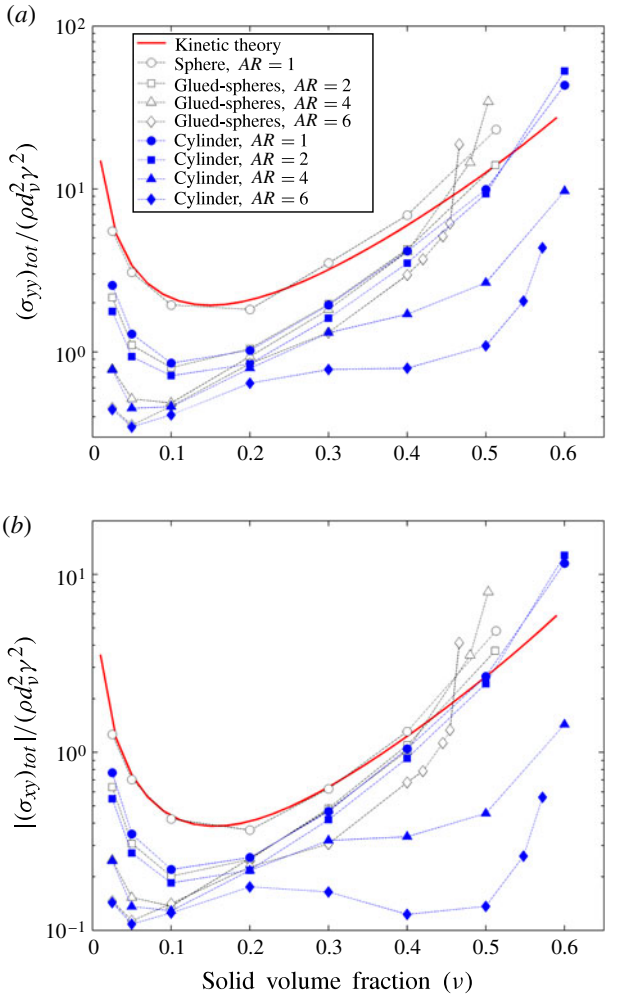


FIGURE 6. (Colour online) Total values of the normalized normal stresses (*a*) and shear stresses (*b*) as a function of solid volume fraction (ν).

intermediate regime, which is a transition between the dilute and dense regimes. In this regime, the kinetic and collisional components are comparable, and the stresses initially decrease and then increase with increasing solid volume fraction.

In the present simulations of elongated particles, it is found that the stress tensor is essentially symmetric (the ratio of the difference to the average of the off-diagonal components, $2|\sigma_{xy} - \sigma_{yx}|/(\sigma_{xy} + \sigma_{yx})$, is below 1 %). Under the condition of symmetry of the stress tensor, the Cosserat continuum models (Mitarai, Hayakawa & Nakanishi 2002; Mohan, Rao & Nott 2002) predict that the mean angular velocity of the particles is equal to the local rate of rotation of the mean flow, i.e. half the local vorticity of the stream. However, this prediction is not true for the non-spherical particles considered in this study. The present simulation results show that at low solid volume fractions ($\nu < 0.2$), the mean particle angular velocity (in the z direction) increases as the particle aspect ratio increases, and the mean angular velocity of particles with large aspect ratios of $AR = 4$ and 6 can be greater than half the vorticity of the mean

https://doi.org/10.1017/jfm.2012.423 Published online by Cambridge University Press

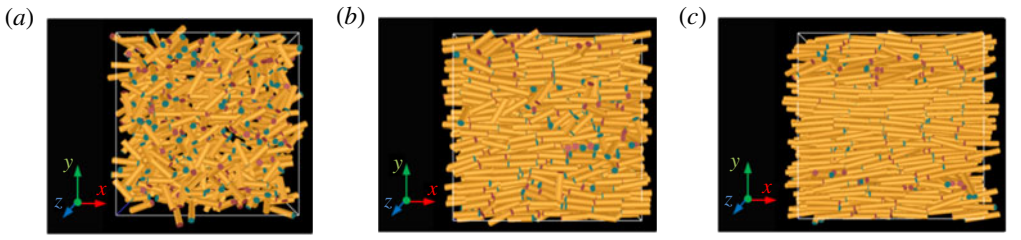


FIGURE 7. (Colour online) Snapshots of shear flows of true cylindrical particles at steady state: (*a*) $AR = 4$, $\nu = 0.2$; (*b*) $AR = 4$, $\nu = 0.6$; (*c*) $AR = 6$, $\nu = 0.572$.

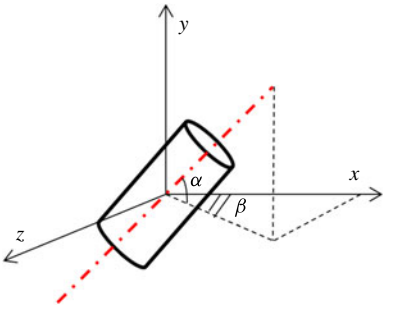


FIGURE 8. (Colour online) Description of particle orientation using the angles α and β.

flow (i.e. 0.5γ) by a factor of more than 2. At high solid volume fractions ($\nu > 0.3$), due to the significant particle alignment with large particle aspect ratios ($AR = 4$ and 6), the rotational motion of particles is markedly resisted. Thus, the angular velocities of the large aspect ratio particles are much lower than half the vorticity. The decrease in angular velocity due to the particle alignment was also observed by Reddy *et al.* (2010) in their hard-particle DEM modelling of two-dimensional shear flows of elongated dumbbell-shaped particles. As a result, the Cosserat continuum models proposed by Mitarai *et al.* (2002) and Mohan *et al.* (2002) may not be used to describe the flow of anisotropic particles with large aspect ratios.

3.2. *Preferred particle orientation*

Several snapshots of the shear flow of cylindrical particles at steady state are shown in figure 7, in which the particles flow in the x direction and a linear x-velocity profile is assigned in the y direction (see also figure 2). For the system with the particle aspect ratio of $AR = 4$ and the solid fraction of $\nu = 0.2$ (figure 7*a*), the orientations of the particles are fairly random. However, with the same particle aspect ratio but a larger solid volume fraction of $\nu = 0.6$ (figure 7*b*), a large number of particles have their major axes aligned horizontally in the flow direction (i.e. the x direction). This orientational preference becomes more significant as the particle aspect ratio increases to six and with a relatively large solid volume fraction (figure 7*c*).

Regardless of the rotation about the major axis, the orientation of a particle can be described by two angles α and β, as shown in figure 8, where α represents the angle between the major axis and its projection onto the horizontal plane (x–z plane) and β is the angle between the projection and the x-axis (in the flow direction). To cover the

https://doi.org/10.1017/jfm.2012.423 Published online by Cambridge University Press

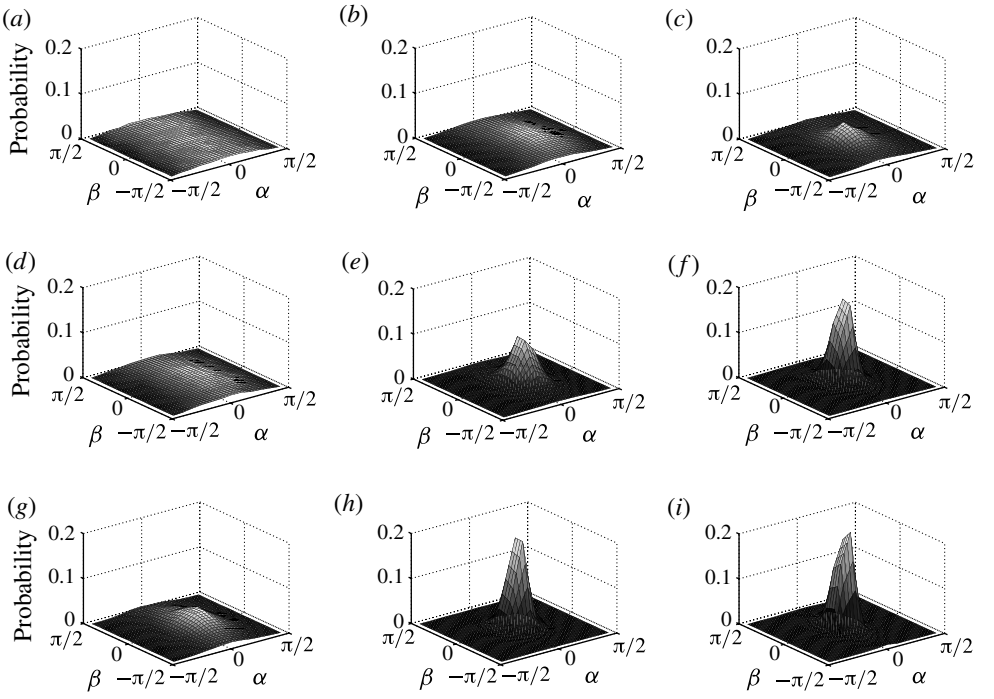


FIGURE 9. Time-averaged results of the particle orientation probability distribution as a function of α and β (true cylindrical particles): (*a*) $AR = 2$, $\nu = 0.2$; (*b*) $AR = 2$, $\nu = 0.4$; (*c*) $AR = 2$, $\nu = 0.6$; (*d*) $AR = 4$, $\nu = 0.2$; (*e*) $AR = 4$, $\nu = 0.4$; (*f*) $AR = 4$, $\nu = 0.6$; (*g*) $AR = 6$, $\nu = 0.2$; (*h*) $AR = 6$, $\nu = 0.4$; (*i*) $AR = 6$, $\nu = 0.572$.

entire space, α should run between $\pm\pi/2$ and β should run between $\pm\pi$. However, due to the geometric symmetry of the particle, one end of the cylindrical particle cannot be distinguished from the other, so both α and β are limited in the range between $\pm\pi/2$. Figure 9 shows the probability distributions of particle orientation as a function of α and β for a variety of particle aspect ratios (AR) and solid volume fractions (ν). The particle orientation probability distributions are time-averaged over the steady state period. As shown in figure 9, with a small aspect ratio and a low solid volume fraction (say $AR = 2$ and $\nu = 0.2$), a relatively uniform probability distribution is obtained over a large range of α and β. As the solid volume fraction increases and/or the particle aspect ratio increases, a significantly high probability is obtained with α and β confined in narrow ranges around zero, indicating that particles are preferentially aligned with the major axes towards the flow direction. In a dilute system, a large space is available for the particles to move and rotate, so the particles have random orientations. As the solid volume fraction increases, the particles collide with their neighbours more frequently and less space is allowed for the particles to rotate, particularly for the particles with large aspect ratios. This constraint results in the aforementioned particle alignment, by which the interference of particles with the bulk flow is minimized.

Time-averaged profiles of particle orientation probability distributions for the true cylindrical particles as a function of α, for a variety of particle aspect ratios and solid volume fractions, are plotted in figure 10. In general, as α approaches zero,

https://doi.org/10.1017/jfm.2012.423 Published online by Cambridge University Press

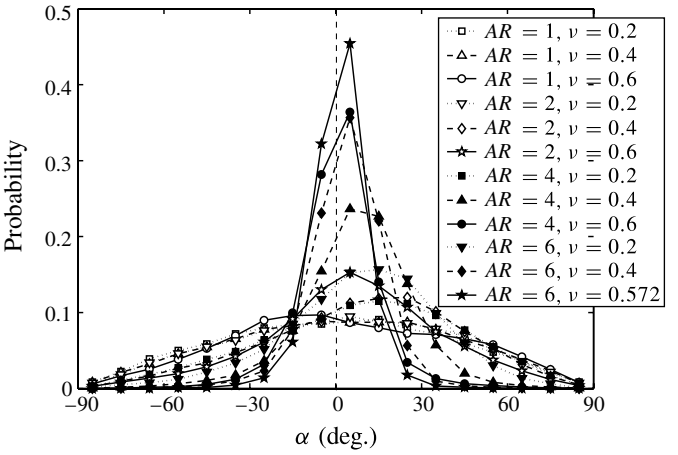


FIGURE 10. Time-averaged profiles of particle orientation probability distribution as a function of α for true cylindrical particles.

the probability increases. As the particle aspect ratio and/or the solid volume fraction increases, the large probability region becomes narrower and the maximum value of the probability increases, indicating that a larger percentage of particles align with the major axes in the flow direction. In addition, for granular systems with large particle aspect ratios and large solid volume fractions, the maximum values of probability are found at small and positive α in the range 0 and 10°. The phenomenon that elongated particles have preferred inclination angles in shear flows was also observed in the simulations of ellipsoidal particles by Campbell (2011).

The particle orientation preference was also examined for shear flows of the glued-spheres particles. Similar probability distribution profiles were obtained for the glued-spheres particle systems and true cylindrical particle systems with the same particle aspect ratios and solid volume fractions, as illustrated in figure 11. Therefore, compared to the effects of the particle aspect ratio and solid volume fraction, the effect of the particle surface roughness has a less significant impact on the particle alignment behaviour in shear flows.

3.3. *Effective projected area*

As shown in figure 7, a particle with larger projected area in the y–z plane has a greater chance of colliding with neighbouring particles. In this study, for a steady shear flow, the projected lengths of a particle in the y and z directions are given as h and w, respectively, in which h represents the difference between the maximum and minimum y-coordinates of the points within the projected area in the y–z plane and similarly w is the difference between the maximum and minimum z-coordinates. Given the particle length, diameter and orientation information (i.e. the angles α and β as illustrated in figure 8), h and w can be obtained for each individual particle. Hence, the product of the average values $\langle h \rangle$ and $\langle w \rangle$ is defined as the effective projected area in the y–z plane having the form

$$S_{eff} = \langle h \rangle \, \langle w \rangle. \tag{3.1}$$

Figure 12 shows the normalized effective projected area, A_{eff}, as a function of the solid volume fraction for the glued-spheres and cylindrical particle systems for a variety of

https://doi.org/10.1017/jfm.2012.423 Published online by Cambridge University Press

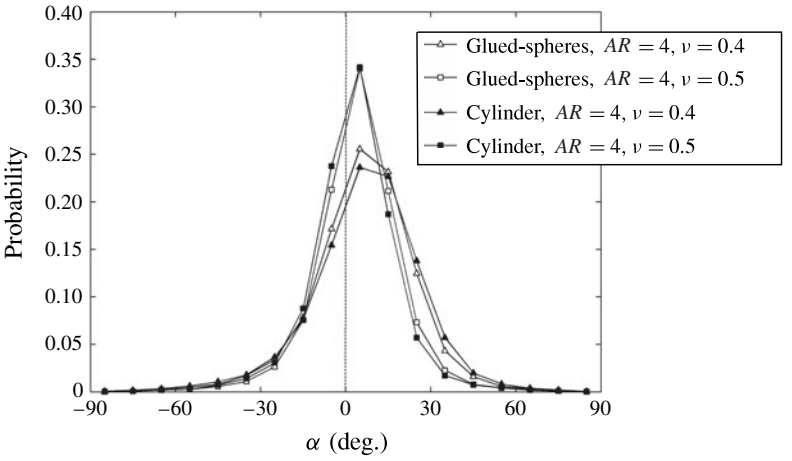


FIGURE 11. Comparison of orientation probability distributions between glued-spheres particles and cylindrical particles.

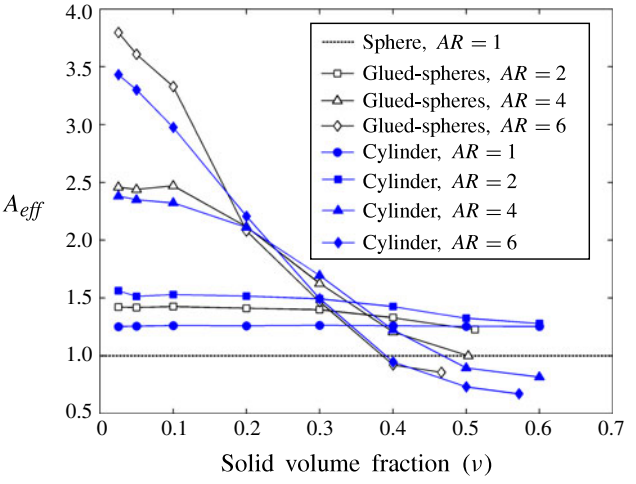


FIGURE 12. (Colour online) Variation of normalized effective projected area with solid volume fraction (ν).

particle aspect ratios. The normalized effective projected area is given by

$$A_{eff} = \frac{S_{eff}}{S_{sph}}, \tag{3.2}$$

in which S_{sph} is the effective projected area of an equivalent volume sphere. Hence, for spherical particles, A_{eff} is always equal to 1. As shown in figure 12, for the small particle aspect ratios ($AR = 1$ and 2), A_{eff} changes only slightly with the solid volume fraction. However, with the larger aspect ratios ($AR = 4$ and 6), a strong dependence of A_{eff} on the solid volume fraction is observed. Large effective projected areas are obtained at low solid volume fractions ($\nu \leqslant 0.1$). The projected areas decrease quickly as the solid volume fraction increases from 0.1 to 0.5, and then decrease slowly at

https://doi.org/10.1017/jfm.2012.423 Published online by Cambridge University Press

high solid volume fractions ($\nu > 0.5$). At low solid volume fractions, abundant space is available for the particles to rotate; therefore, the effective projected area increases with increasing particle aspect ratio, which increases the length of a particle (by fixing the particle volume). However, at high solid volume fractions, the particles with large aspect ratios have a preferred orientation with the major axes of particles aligned nearly parallel to the flow direction, as discussed in § 3.2. This particle alignment causes a decrease in the effective projected area. As a result, at high solid volume fractions ($\nu > 0.4$), the effective projected area decreases with increasing particle aspect ratio.

3.4. *Stresses in dilute granular systems*

For a dilute granular system, the main contributor to its stress is the kinetic component, which is proportional to the particle fluctuating velocity squared. The fluctuating velocity is proportional to the time between two consecutive collisions, which is inversely proportional to the particle collision frequency. The particle collision frequency is believed to be proportional to the particle's effective projected area in the plane perpendicular to the flow direction (see also Reddy *et al.* 2010). Based on these analyses, the following relationship can be obtained:

$$\boldsymbol{\sigma} \propto \frac{1}{(A_{eff})^2}. \tag{3.3}$$

Figure 13 shows the normalized stresses as a function of $(A_{eff})^{-2}$ for the dilute granular systems. The stress results for the frictionless spherical particle system, glued-spheres particle systems, and cylindrical particle systems, with various particle aspect ratios and a variety of solid volume fractions, are presented. For the non-spherical particle systems (i.e. glued-spheres and cylindrical particle systems), a linear relationship is obtained at the solid volume fractions of $\nu = 0.025$, 0.05, and 0.1. It should be noted that the stress results for the spherical particle systems ($A_{eff} = 1$) fall above the corresponding inclined lines determined by the non-spherical particle systems with the same solid volume factions (ν). This behaviour is due to the rotational motion of the non-spherical particles, which increases the rate of dissipation of the translational energy and therefore leads to smaller stresses, as discussed in § 3.1. For the system with the solid volume fraction of $\nu = 0.2$, a linear relationship is no longer obtained. This is due to the more frequent interparticle collisions and the significant contribution of collisional stresses in a denser system.

Due to the linear relationship between the normalized stresses and $(A_{eff})^{-2}$ for the dilute, non-spherical particle systems, one might be able to incorporate the term $(A_{eff})^{-2}$ into the kinetic theory model (Lun *et al.* 1984) as follows:

$$\frac{\sigma_{yy}}{\rho d_v^2 \gamma^2} = \frac{k_{yy}}{(A_{eff})^2} \sigma_{yy}^N(\nu, e), \tag{3.4}$$

$$\frac{\sigma_{xy}}{\rho d_v^2 \gamma^2} = \frac{k_{xy}}{(A_{eff})^2} \sigma_{xy}^N(\nu, e), \tag{3.5}$$

in which $\sigma_{yy}^N(\nu, e)$ and $\sigma_{xy}^N(\nu, e)$ are expressed as (1.7) and (1.8), respectively. The normalized effective projected area, A_{eff}, accounts for the effect of particle shape (e.g. particle aspect ratio). In addition, k_{yy} and k_{xy} are two parameters which account for the effect of particle rotation on the rate of dissipation of translational energy. If the particles are spherical and frictionless, A_{eff} is equal to one, and k_{yy} and k_{xy} are both

https://doi.org/10.1017/jfm.2012.423 Published online by Cambridge University Press

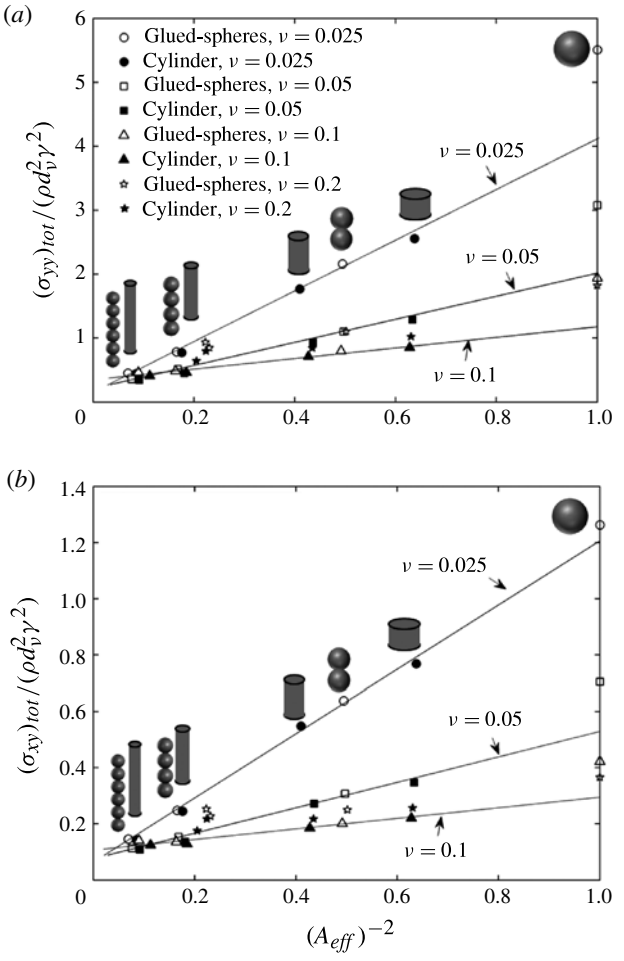


FIGURE 13. Normalized normal stresses (*a*) and shear stresses (*b*) as a function of $(A_{eff})^{-2}$ for the dilute granular systems at different solid volume fractions.

equal to one without particle rotation, allowing (3.4) and (3.5) to return to (1.7) and (1.8).

To verify the new stress descriptions ((3.4) and (3.5)) for the dilute non-spherical particle systems, the normalized normal and shear stresses are plotted in figure 14 as a function of $\sigma_{yy}^N(\nu, e)\,(A_{eff})^{-2}$ and $\sigma_{xy}^N(\nu, e)\,(A_{eff})^{-2}$, respectively, for the glued-spheres and cylindrical particle systems with low solid volume fractions. These stress results with the solid volume fractions of 0.025, 0.05 and 0.1 collapse onto two straight lines. The slopes of the lines, $k_{yy} = 0.6$ and $k_{xy} = 0.74$, are less than one, indicating a reduction in the stresses due to the loss of the translational energy to rotational energy for the non-spherical particle systems. It can be seen from figure 14 that the stress results with a relatively high solid volume fraction of 0.2 show a deviation from the collapsed lines, particularly for the glued-spheres particles. This deviation is caused by the significant collisional contribution to the stresses in a moderately dense system. In addition, the bumpy and rough surfaces of the glued-spheres particles can also

https://doi.org/10.1017/jfm.2012.423 Published online by Cambridge University Press

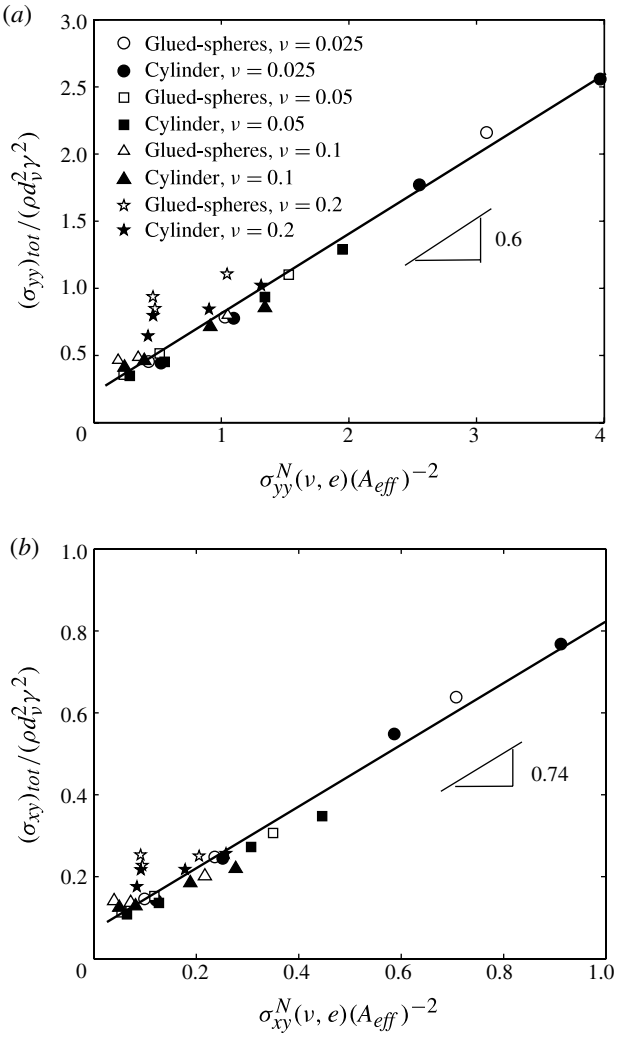


FIGURE 14. Collapse of the normal stresses (*a*) and shear stresses (*b*) in the dilute systems of glued-spheres and cylindrical particles.

promote the particle–particle interactions in a dense flow, which will be discussed in the following section.

3.5. *Effect of particle surface roughness*

The elongated particles formed by gluing spheres have bumpier bands compared to the true cylindrical particles as shown in figure 1. During shear flows at high solid volume fractions, strong interactions occur due to the rough surfaces for the glued-spheres particles when one particle slides past another, as illustrated in figure 15. This interaction can potentially increase the contact number and contact forces, leading to larger stresses. To examine this hypothesis, the dimensionless contact number densities are plotted as a function of the particle aspect ratio for the glued-spheres and cylindrical particles in figure 16, where the dimensionless contact number density is defined as the number of interparticle contacts per unit volume scaled by the cube

https://doi.org/10.1017/jfm.2012.423 Published online by Cambridge University Press

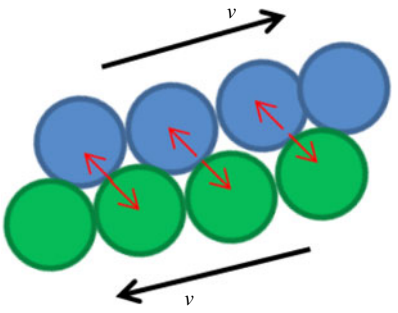


FIGURE 15. (Colour online) Illustration of the interaction between two rough glued-spheres particles when they pass each other.

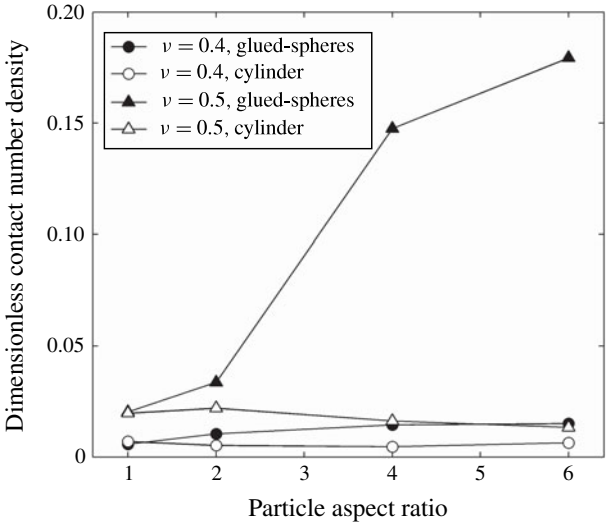


FIGURE 16. Dimensionless contact number densities as a function of the particle aspect ratio for the glued-spheres and true cylindrical particles.

of the particle equivalent diameter (d_v^3). For the true cylindrical particles, the contact number density increases as the solid volume fraction increases, but it decreases slightly with increasing particle aspect ratio due to the alignment of large aspect ratio particles. For the glued-spheres particles, the contact number density increases as the particle aspect ratio increases, due to the increase in the number of the constituent spheres in a single particle. In addition, a particle with a bumpy surface, driven by strong interparticle collisions, rotates its long axis and thus increases its likelihood of contacting other particles. The contact number density for the glued-spheres particles also increases with increasing solid volume fraction, and sharp increases are obtained at large particle aspect ratios ($AR = 4$ and 6). This increase in contact number density leads to the sharp increases in the stresses that are observed with the glued-spheres particles with large particle aspect ratios ($AR = 4$ and 6) at the high solid volume fractions ($0.4 < \nu < 0.5$), as shown in figure 6.

https://doi.org/10.1017/jfm.2012.423 Published online by Cambridge University Press

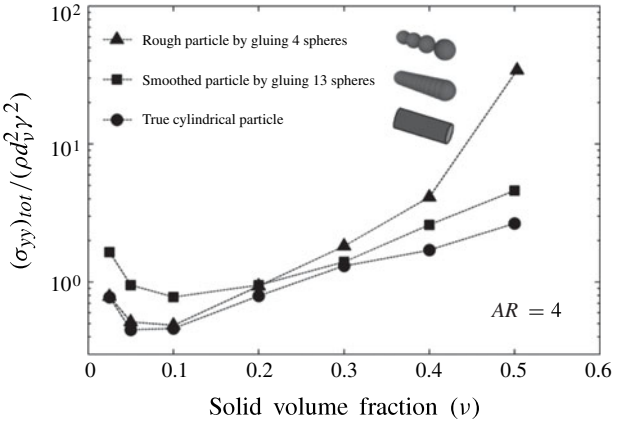


FIGURE 17. Comparison of stresses with rough glued-spheres particles, smoothed glued-spheres particles, and cylindrical particles.

As pointed by Abbaspour-Fard (2004), the bumpy surfaces of the glued-spheres particles had the same effect as friction on the movement of particles, so that the effect of these rough surfaces was termed 'pseudo-friction'. His DEM simulation results showed that the 'pseudo-friction' decreases as the surface of a glued-spheres particle becomes smoother by using more constituent spheres, which overlap one another. Figure 17 shows a comparison of the normalized normal stresses for rough glued-spheres, smoothed glued-spheres, and true cylindrical particle systems, in which the particle aspect ratio is fixed at $AR = 4$. A single rough glued-spheres particle is generated by gluing four identical spheres in a straight line without overlap, and a smoothed glued-spheres particle is generated by gluing 13 constituent spheres, the centres of which are uniformly distributed in a line with two neighbour spheres overlapped. The results show that at the high solid volume fractions, the highest stresses are obtained for the rough glued-spheres particles and the lowest stresses are obtained for the true cylindrical particle. The stresses for the smoothed glued-spheres particles fall in between these two cases. Therefore, it is evident that the stresses may increase as the surfaces of particles become rougher in a dense granular system due to the increased contact number and enhanced interactions with the rough surfaces.

3.6. *Apparent friction coefficient*

The ratio of the magnitudes of the shear to normal stresses, $|\sigma_{xy}|/\sigma_{yy}$, is referred to as the apparent friction coefficient, which indicates the macroscopic friction coefficient of the bulk granular material. Figure 18 shows the apparent friction coefficients as a function of the solid volume fraction for the glued-spheres and cylindrical particle systems with a variety of particle aspect ratios. The simulation results for the frictionless spherical particles are in good agreement with the prediction of kinetic theory (Lun *et al.* 1984). The apparent friction coefficient initially decreases and then increases with increasing solid volume fraction. For the particles with small particle aspect ratios ($AR = 1$ and 2), the trends of the apparent friction coefficient varying solid volume fraction follow a similar shape as that of the spheres. However, the apparent friction coefficients of the glued-spheres and cylindrical particle systems with small particle aspect ratios are larger than those of the spherical particle system, due to the loss of translational energy to rotational energy.

https://doi.org/10.1017/jfm.2012.423 Published online by Cambridge University Press

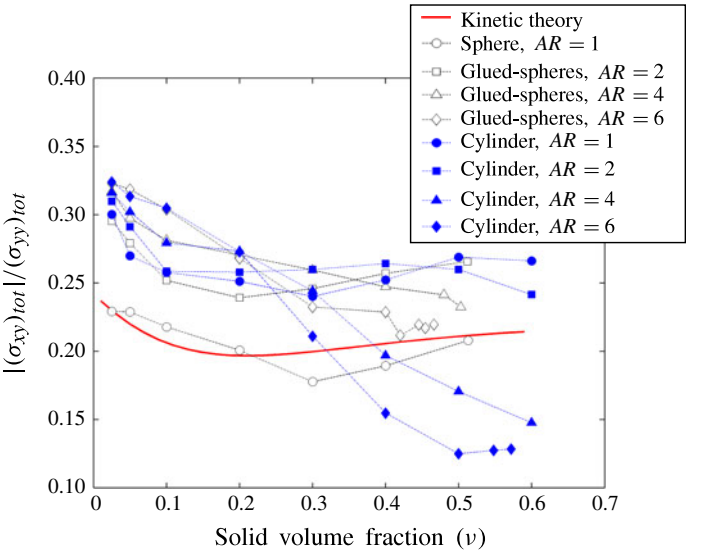


FIGURE 18. (Colour online) Apparent friction coefficients as a function of the solid volume fraction for the glued-spheres and cylindrical particle systems with a variety of particle aspect ratios.

For the particles with large particle aspect ratios ($AR = 4$ and 6), the apparent friction coefficient generally decreases as the solid volume fraction increases. This decrease is due to the strong alignment of the particles' major axes towards the flow direction in dense systems of elongated particles (figures 7 and 9). At low solid volume fractions ($\nu \leqslant 0.2$), the apparent friction coefficients are nearly the same for the glued-spheres particles and the cylindrical particles given the same particle aspect ratio ($AR = 4$ or 6). However, the apparent friction coefficients with the cylindrical particles are much lower than with the glued-sphere particles at relatively high solid fractions ($\nu > 0.3$). This difference is attributed to the different surface properties between the true cylindrical and glued-spheres particles. The smooth surfaces of the cylindrical particles can reduce or avoid the interlocking of particles that is present with glued-spheres and consequently facilitate particles sliding past each other, thus leading to a decrease in the apparent friction coefficient.

4. Conclusions

The main contribution of this work is that the stress results are obtained for the shear flows of large aspect ratio particles with bumpy and smooth surfaces by performing three-dimensional DEM simulations of glued-spheres and true cylindrical particles. Based on these stress results, the effect of particle shape, in terms of particle aspect ratio and surface roughness, on the granular flow behaviour and constitutive relations is systematically explored. Some major conclusions are drawn as follows.

4.1. *The effect of particle aspect ratio*

Three distinct regimes have been discerned for the granular flows based on the solid volume fraction (ν): the dilute regime, the dense regime, and an intermediate regime. In the dilute regime ($\nu < 0.1$ for $AR = 1$ and 2; $\nu < 0.05$ for $AR = 4$ and 6), kinetic stresses are dominant and momentum is transferred mainly by particle movement.

https://doi.org/10.1017/jfm.2012.423 Published online by Cambridge University Press

Therefore, the trends of total stresses in this regime follow the same shapes as their kinetic components. In this regime, similar stresses are obtained for the glued-spheres and true cylindrical particles given the same particle aspect ratio, except for $AR = 1$. In addition, the stresses decrease as the particle aspect ratio increases, due to the decrease in the mean free path length and the loss of translational energy to rotational energy.

In the dense regime ($\nu > 0.2$), collisional stresses are dominant and momentum is transferred mainly by interparticle collisions. Thus, the trends of total stresses in this regime follow the same shapes as their collisional components. In this regime, stresses for all the granular systems with small particle aspect ratios ($AR = 1$ and 2) follow the same trend. For the glued-spheres particles with large particle aspect ratios ($AR = 4$ and 6), a sharp increase in the stresses with increasing ν is observed, due to the effect of the bumpy surfaces of particles. However, in the dense regime, much smaller stresses are obtained for the true cylindrical particles with $AR = 4$ and 6 compared to the true cylindrical particles with small particle aspect ratios and all the glued-spheres particles considered. This behaviour is likely due to the combined effects of the smooth surfaces of the cylindrical particles and the alignment of particles in a manner such that their major axes are aligned towards the flow direction. Between the dilute and dense regimes is the intermediate regime, in which the kinetic and collisional components are comparable, and a transition from a stress decrease to an increase occurs with increasing ν in this regime.

For dilute shear flows of granular materials ($\nu < 0.1$), the effective particle projected area on the plane perpendicular to the flow direction, which increases as the particle aspect ratio increases, affects the stresses by determining the probability of particle collisions. Thus, the kinetic theory model (Lun *et al.* 1984) is modified by incorporating the normalized effective particle projected area (A_{eff}) to describe the stresses for dilute granular flows of the non-spherical particles. In dense flows, the preferred orientation of the particles minimizes the particles' projected area and thus the interference with the flow is minimized. This orientational preference becomes more significant as the particle aspect ratio increases and/or the solid volume fraction increases.

4.2. *The effect of particle surface geometry*

By using two different types of particles (i.e. glued-spheres particles and true cylindrical particles), the effect of particle surface geometry has been investigated. In general, smaller stresses are obtained with the non-spherical particles compared to the spherical particles in dilute and moderately dense flows ($\nu < 0.4$) due to the occurrence of rotation of the non-spherical particles. Compared to the effect of the particle aspect ratio, the particle surface geometry has a limited influence on the stresses for dilute systems ($\nu < 0.1$) of elongated particles ($AR \geqslant 2$). However, the particle aspect ratio has a significant impact on the stresses in dense granular flows with large particle aspect ratios ($AR = 4$ and 6). In dense flows, as particles slide past the surfaces of their neighbours, many more interparticle collisions occur simultaneously with the bumpy glued-spheres particles rather than with the smooth cylindrical particles. Hence, the stresses increase as the particle surfaces become bumpier or rougher.

The apparent friction coefficient depends on the particle aspect ratio and the surface roughness. A rapid decrease in the apparent friction coefficient with increasing solid volume fraction is observed for the true cylindrical particles with large aspect ratios ($AR = 4$ and 6). This decrease is due to the combined effects of the strong particle alignment and the smooth bands of the elongated particles.

https://doi.org/10.1017/jfm.2012.423 Published online by Cambridge University Press

4.3. *Implication for the future work*

It is clear that particle shape and surface geometry have a strong impact on the stresses and rheology of granular shear flows. In this work, we have considered frictionless, rod-like particles. In future work, other shapes such as low aspect ratio disks will be investigated to provide more information on the effect of particle shape. Also, the effect of interparticle friction and particle elasticity on the flows of non-spherical particles will be studied in depth. Based on these studies, a more comprehensive kinetic theory may be developed for the dilute and dense flows of non-spherical particles, taking into account the effects of particle shape and material properties.

Acknowledgements

This research is based on the funding from NSF-CBET Grant No. 0854005, from NASA-STTR Phase II Program, and from the State of Florida Space Research Initiative. The authors also acknowledge the University of Florida High-Performance Computing Center for providing computational resources.

REFERENCES

ABBASPOUR-FARD, M. H. 2004 Theoretical validation of a multi-sphere, discrete element model suitable for biomaterials handling simulation. *Biosystems Engineering* **88** (2), 153–161.

BERZI, D., DI PRISCO, C. G. & VESCOVI, D. 2011 Constitutive relations for steady, dense granular flows. *Phys. Rev.* E **84**, 031301.

CAMPBELL, C. S. 1989 The stress tensor for simple shear flows of a granular material. *J. Fluid Mech.* **203**, 449–473.

CAMPBELL, C. S. 2002 Granular shear flows at the elastic limit. *J. Fluid Mech.* **465**, 261–291.

CAMPBELL, C. S. 2005 Stress-controlled elastic granular shear flows. *J. Fluid Mech.* **539**, 273–297.

CAMPBELL, C. S. 2006 Granular material flows: an overview. *Powder Technol.* **162**, 208–229.

CAMPBELL, C. S. 2011 Elastic granular flows of ellipsoidal particles. *Phys. Fluids* **23**, 013306.

CAMPBELL, C. S. & GONG, A. 1986 The stress tensor in a two-dimensional granular shear flow. *J. Fluid Mech.* **164**, 107–125.

CARNAHAN, N. F. & STARLING, K. E. 1969 Equation of state for nonattracting rigid spheres. *J. Chem. Phys.* **51**, 635–636.

CLEARY, P. W. 2008 The effect of particle shape on simple shear flows. *Powder Technol.* **179**, 144–163.

CLEARY, P. W. & SAWLEY, M. L. 2002 DEM modeling of industrial granular flows: 3D case studies and the effect of particle shape on hopper discharge. *Appl. Math. Model.* **26**, 89–111.

CUNDALL, P. A. & STRACK, O. D. L. 1979 A discrete numerical model for granular assemblies. *Geotechnique* **29**, 47–65.

FORTERRE, Y. & POULIQUEN, O. 2008 Flows of dense granular media. *Annu. Rev. Fluid Mech.* **40**, 1–24.

GOLDSHTEIN, A. & SHAPIRO, M. 1995 Mechanics of collisional motion of granular materials. Part 1. General hydrodynamic equations. *J. Fluid Mech.* **282**, 75–114.

GUO, Y., WASSGREN, C., KETTERHAGEN, W., HANCOCK, B. & CURTIS, J. 2012 Some computational considerations associated with discrete element modelling of cylindrical particles. *Powder Technol.* **228**, 193–198.

HERTZ, H. 1882 Über die Berührung fester elastischer Körper. *J. Reine Angew. Math.* **92**, 156–171.

JENKINS, J. T. 2006 Dense shearing flows of inelastic disks. *Phys. Fluids* **18**, 103307.

JENKINS, J. T. & RICHMAN, M. W. 1985 Kinetic theory for plane flows of a dense gas of identical, rough, inelastic, circular disks. *Phys. Fluids* **28** (12), 3485–3494.

JENKINS, J. T. & ZHANG, C. 2002 Kinetic theory for identical, frictional, nearly elastic spheres. *Phys. Fluids* **14** (3), 1228–1235.

https://doi.org/10.1017/jfm.2012.423 Published online by Cambridge University Press

JOHNSON, P. C. & JACKSON, R. 1987 Frictional–collisional constitutive relations for granular materials with applications to plane shearing. *J. Fluid Mech.* **176**, 67–93.

JOHNSON, P. C., NOTT, P. & JACKSON, R. 1990 Frictional–collisional equations of motion for particulate flows and their applications to plane shearing. *J. Fluid Mech.* **210**, 501–535.

KETTERHAGEN, W. R., CURTIS, J. S. & WASSGREN, C. R. 2005 Stress results from two-dimensional granular shear flow simulations using various collision models. *Phys. Rev.* E **71**, 061307.

KODAM, M., BHARADWAJ, R., CURTIS, J., HANCOCK, B. & WASSGREN, C. 2010*a* Cylindrical object contact detection for use in discrete element method simulations. Part 1. Contact detection algorithms. *Chem. Engng Sci.* **65**, 5852–5862.

KODAM, M., BHARADWAJ, R., CURTIS, J., HANCOCK, B. & WASSGREN, C. 2010*b* Cylindrical object contact detection for use in discrete element method simulations. Part 2. Experimental validation. *Chem. Engng Sci.* **65**, 5863–5871.

LASINSKI, M. E., CURTIS, J. S. & PEKNY, J. F. 2004 Effect of system size on particle-phase stress and microstructure formation. *Phys. Fluids* **16** (2), 265–272.

LEES, A. W. & EDWARDS, S. F. 1972 The computer study of transport processes under extreme conditions. *J. Phys. C: Solid State Phys.* **5**, 1921–1929.

LUN, C. K. K., SAVAGE, S. B., JEFFREY, D. J. & CHEPURNIY, N. 1984 Kinetic theories for granular flow: inelastic particles in Couette flow and slightly inelastic particles in a general flow field. *J. Fluid Mech.* **140**, 223–256.

MITARAI, N., HAYAKAWA, H. & NAKANISHI, H. 2002 Collisional granular flow as a micropolar fluid. *Phys. Rev. Lett.* **88**, 174301.

MOHAN, L. S., RAO, K. K. & NOTT, P. R. 2002 A frictional Cosserat model for the slow shearing of granular materials. *J. Fluid Mech.* **457**, 377–409.

MONTANERO, J. M., GARZO, V., SANTOS, A. & BREY, J. J. 1999 Kinetic theory of simple granular shear flows of smooth hard spheres. *J. Fluid Mech.* **389**, 391–411.

PEÑA, A. A., GARCÍA-ROJO, R. & HERRMANN, H. J. 2007 Influence of particle shape on sheared dense granular media. *Granul. Matt.* **9**, 279–291.

REDDY, K. A., KUMARAN, V. & TALBOT, J. 2009 Orientational ordering in sheared inelastic dumbbells. *Phys. Rev.* E **80**, 031304.

REDDY, K. A., TALBOT, J. & KUMARAN, V. 2010 Dynamics of sheared inelastic dumbbells. *J. Fluid Mech.* **660**, 475–498.

WALTON, O. R. & BRAUN, R. L. 1986 Viscosity, granular-temperature, and stress calculations for shearing assemblies of inelastic, frictional disks. *J. Rheol.* **30** (5), 949–980.

YOON, D. K. & JENKINS, J. T. 2005 Kinetic theory for identical, frictional, nearly elastic disks. *Phys. Fluids* **17**, 083301.

https://doi.org/10.1017/jfm.2012.423 Published online by Cambridge University Press